THE JOURNAL OF PHYSICAL CHEMISTRY C

Article

Cite This: J. Phys. Chem. C 2018, 122, 19712−19721

pubs.acs.org/JPCC

Copper Dimer Supported on a C_2N Layer as an Efficient Electrocatalyst for CO_2 Reduction Reaction: A Computational Study

Jia Zhao,[†] Jingxiang Zhao,*[,†] Fengyu Li,[‡] and Zhongfang Chen*[,§]

[†]College of Chemistry and Chemical Engineering, and Key Laboratory of Photonic and Electronic Bandgap Materials, Ministry of Education, Harbin Normal University, Harbin 150025, China

[‡]School of Physical Science and Technology, Inner Mongolia University, Hohhot 010021, China

[§]Department of Chemistry, University of Puerto Rico, Rio Piedras Campus, San Juan, Puerto Rico 00931, United States

Supporting Information

ABSTRACT: The carbon dioxide electrochemical reduction (CO_2RR) to useful fuels and chemicals with renewable electricity offers a promising strategy for resolving energy security and environmental issues. Searching for low-cost catalysts with high efficiency and high selectivity is crucial to achieve this goal. Here, by means of comprehensive density functional theory computations, we systematically investigated the potential of several transition metal dimers supported on a porous C_2N layer ($Cu_2@C_2N$) as the CO_2RR electrocatalysts. Our results revealed that the Cu dimer can be stably embedded in the porous C_2N monolayer because of the strong hybridization between Cu 3d orbitals and N 2p orbitals, thus ensuring its high stability. On the basis of the computed free energy changes, we found that $Cu_2@C_2N$ exhibits superior performance for the CO_2RR with a small limiting potential of −0.23 V and the $CO_2 \rightarrow HCOO^* \rightarrow HCOOH^* \rightarrow H_2COOH^* \rightarrow H_2CO^* \rightarrow H_2COH^* \rightarrow CH_2^* \rightarrow CH_3^* \rightarrow CH_4$ route is the most favorable, among which the hydrogenation of HCOO* to HCOOH* is the potential-determining step. In addition, C_2H_4 can also be yielded as the formed CO* provides active sites for the coupling with another CO species with the limiting potential of −0.76 V. Therefore, $Cu_2@C_2N$ layer is a quite promising bi-atom catalyst for the electrochemical reduction of CO_2 to hydrocarbons.

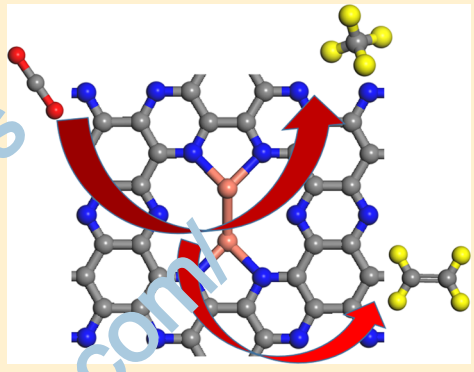

1. INTRODUCTION

In recent years, the CO_2 electroreduction reaction (CO_2RR) to useful fuels and value-added chemicals using electricity generated from renewable sources, such as sunlight and wind, has gained considerable research interest since the ever increasing CO_2 emission from the unprecedented combustion of fossil fuels poses a severe threat to the global environment.[1] However, efficient, stable, and inexpensive catalysts for the CO_2RR are highly desired because of the extremely thermodynamic stability of CO_2 molecule. Past years have witnessed tremendous efforts toward developing efficient and less-energy-intensive CO_2RR catalysts. To date, various transition metals (TMs) (i.e., Cu, Ag, Fe, Ni, and Au) have been widely utilized as electrocatalysts for CO_2RR;[8] especially the copper catalysts, first proposed by Hori et al.,[9] have demonstrated their unique performance in reducing CO_2 to hydrocarbons, mainly CH_4, C_2H_4, CO, and HCOOH. However, the electrocatalytic performance of Cu is still unsatisfactory because of several fundamental challenges, such as the high overpotential (∼1 V) and low faradaic efficiency as a result of the competitive hydrogen evolution reaction (HER).[10,11] Hence, during the last few decades, numerous studies have been devoted to enhance the CO_2RR catalytic performance by tuning the structures of Cu electrocatalysts, including Cu-based alloys,[12,13] Cu nanowires,[14−17] O- or S-derived Cu,[18−22] and Cu nanoparticles supported on carbon-based nanostructures.[23,24] Nevertheless, the activity of the above Cu-based catalysts is strongly dependent on the size, shape, grain boundary, crystal facets, and so on,[25] which would impose extra difficulties in synthetic methods and mechanism analyses. Therefore, downsizing these metal nanostructures to singly dispersed metal atoms is highly desirable for maximizing the efficiency of catalytically active metal sites.

Depositing single metal atoms on a certain substrate with fine dispersion has been revealed to be highly active for a variety of catalytic reactions.[26−37] For example, Zhang and co-workers first demonstrated that the single Pt atom deposited on iron oxide surface can present remarkably high activity toward CO oxidation.[28] Afterward, the catalytic performance of the experimentally available single-atom catalysts on other metal oxides substrates, such as Ru_1/Co_3O_4,[32] Au_1/CeO_2,[33] Ag_1/MgO,[34] has been extensively explored. The successful fabrication of single-atom catalysts also inspired many theoretical efforts to study the corresponding reaction mechanisms.[35−38] For example, Li et al. systemically examined

Received: July 6, 2018
Revised: August 1, 2018
Published: August 7, 2018

DOI: 10.1021/acs.jpcc.8b06494
J. Phys. Chem. C 2018, 122, 19712−19721

the stability and catalytic performance of various FeO_x-supported single-atom catalysts for CO oxidation.[35] Liang et al. demonstrated that Ni_1/FeO_x has a high catalytic activity at room temperature for CO oxidation.[36] In particular, single-atom catalysts have been widely employed for various electrochemical reactions,[39] as they not only minimize materials usage to meet the goal of cost-effective catalysis, but also possess outstanding activity because of their high ratio of low-coordinated metal atoms.

As compared to the single-atom catalysts, using a few metal atoms as active sites was revealed to possess improved catalytic performance because of the synergistic effect of two adjacent adsorption sites.[40,41] For example, Liu et al. showed that Cu_4 cluster supported on Al_2O_3 thin films may be an excellent and efficient catalyst for CO_2 reduction in the presence of hydrogen.[40] Liu et al. theoretically proposed that Fe_3 cluster anchored on the θ-Al_2O_3(010) surface can be utilized as a promising heterogeneous catalyst for ammonia synthesis.[41] Similar improvements have also been observed in metal dimers anchored on an appropriate substrate.[42−45] For example, Matsushita et al. fabricated Mo dimers embedded within the rectangular-shaped expanded phthalocyanines (Pc).[42] He et al. successfully synthesized the Fe dimers embedded into graphene with adjacent single vacancies,[43] while Yan et al. fabricated Pt_2 dimers on graphene using atomic layer deposition that exhibited a ∼17- and 45-fold higher catalytic activity toward hydrolytic dehydrogenation of ammonia borane than isolated sites and nanoparticles.[44] Very recently, Tian et al. successfully synthesized highly dispersed Fe_2 clusters that are supported on mesoporous carbon nitride (mpg-C_3N_4) and demonstrated that the obtained Fe_2/mpg-C_3N_4 samples have superior catalytic performance for alkene epoxidation.[45] Theoretically, Sun and co-workers revealed that the Cu dimers on graphene or Mn dimers on a phthalocyanine sheet exhibit higher catalytic activity than their single-atom counterparts.[46−48]

Very recently, a novel nitrogenated hole graphene, that is, C_2N, was successfully synthesized by a simple bottom-up wet-chemical reaction.[49] Interestingly, a C_2N layer is featured with evenly distributed cavities terminated by sp^2-bonded nitrogen atoms, which can provide coordination sites to anchor metal atoms, since the lone-pair electrons of N atoms can strongly couple with metal atoms and prohibit metal drifting. In addition, a C_2N layer exhibits high thermal stability under air, and has a rather high kinetic stability[50] and high electric conductivity due to its continuous network structure.[49] Quite recently, the catalytic performance of a single metal atom anchored on C_2N monolayers began to attract attention. For example, Li et al. proposed that the single metal atoms anchored on a C_2N monolayer are promising oxygen evolution electrocatalysts[51] and Ma et al. showed that the single Sc, Ti, V, Cr, and Mn atoms embedded into a C_2N monolayer are promising for CO oxidation, while Mo@C_2N possesses good catalytic performance for the ammonia synthesis.[53]

The extensive exploration of a single metal atom supported by a C_2N layer as low-cost, high-performance catalysts and the outstanding catalytic activity of metal dimers inspires us to ask an interesting question: Can the metal dimer supported on a C_2N monolayer be utilized as a good bi-atom catalyst for CO_2RR? Actually, very recent theoretical investigations showed that the dimers of Co, Ni, and Cu atom supported on a C_2N layer present much improved ORR activity as compared with their single-atom counterparts[54] and the Cu dimer supported on a C_2N layer also exhibits much enhanced catalytic performance for CO oxidation.[55]

However, to date the catalytic performance of a TM dimer on C_2N layers toward the CO_2RR has not been addressed experimentally or theoretically. Therefore, a theoretical study on this issue is highly desirable, which will open up a new strategy for developing efficient CO_2RR catalysts with the least metal atoms on porous low-dimensional materials, as the theoretical advances in recent years make it possible to search for efficient catalysts and to describe the corresponding catalytic mechanisms with adequate accuracy.[56,57]

In this work, we systematically studied the potential of a Cu dimer on a C_2N layer (Cu_2@C_2N) as the CO_2RR electrocatalyst under an acidic environment by means of comprehensive density functional theory (DFT) computations. Cu_2@C_2N was selected to study because (1) it has moderate binding strength with the CO_2RR intermediates, as revealed by our screening computations; (2) Cu is the best metal catalyst for CO_2RR reported so far. Our computations demonstrated that Cu_2@C_2N monolayer exhibits excellent CO_2RR catalytic activity with a low limiting potential, in which CH_4 and C_2H_4 are the main products. Therefore, Cu_2@C_2N can be a promising candidate for the next generation of low-cost CO_2RR catalysts with high efficiency and high selectivity.

2. COMPUTATIONAL METHODS

Our spin-polarized DFT computations were performed by using the DMol^3 code.[58,59] The electron interactions were described by Perdew−Burke−Ernzerhof exchange−correlation functional[60] within the generalized gradient approximation. The empirical correction in Grimme's scheme (i.e., DFT + D2)[61] was utilized to treat the (possible) van der Waals interactions between CO_2RR intermediates and catalysts. The relativistic effects of transition metals were considered through the density functional semicore pseudopotential,[62] in which a single effective potential and some degree of relativistic corrections replace the core electrons, while the double numerical plus polarization basis set was used for other elements. Self-consistent field computations were performed with a convergence criterion of 10^{-6} au on the total energy and electronic computations. To ensure high quality results, the real-space global orbital cutoff radius was chosen as high as 5.2 Å in all of the computations.

The Cu_2@C_2N-based catalysts were built by depositing a Cu dimer on a 2 × 2 C_2N supercell containing 24 C, 12 N, and 2 Cu atoms. The vacuum space was set to 20 Å, which was enough to avoid the interactions between periodic images. The Brillouin zone was sampled with a Monkhorst−Pack mesh with a 5 × 5 × 1 grid in reciprocal space during geometry optimizations. The Hirshfeld charge analysis was employed to compute the charge transfer.[63]

The free energy diagrams in the CO_2RR were computed using the computational hydrogen electrode model,[64,65] in which the chemical potential of ($H^+ + e^-$) at pH = 0 is related to the chemical potential of 1 bar H_2 in the gas phase at 298 K. The adsorption energies of CO_2RR intermediates (E_{ads} or ΔE) were first determined according to the following expression: $E_{ads} = E_T - E_{catalyst} - E_{species}$, where E_T, $E_{catalyst}$, and $E_{species}$ are the total energies of an adsorbed system, catalyst, and isolated CO_2RR species, respectively. Furthermore, the Gibbs free energy change (ΔG) can be derived from these adsorption energies as follows: $\Delta G = \Delta E + \Delta ZPE - T\Delta S + \Delta G_U$, where ΔE is obtained directly from DFT calculations, ΔZPE is the

DOI: 10.1021/acs.jpcc.8b06494
J. Phys. Chem. C 2018, 122, 19712−19721

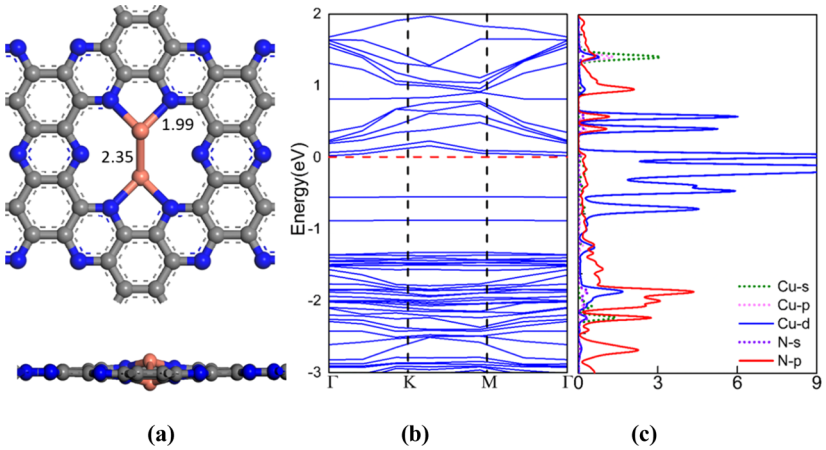

Figure 1. (a) Optimized structure, (b) band structure, and (c) partial density of states (PDOS) of a Cu dimer supported on a porous C_2N layer. The Fermi level was set at 0.

Scheme 1. Proposed Reaction Paths for CO_2 Electrochemical Reduction on Cu-Based Catalysts, Producing Methane (CH_4) and Methanol (CH_3OH)[a]

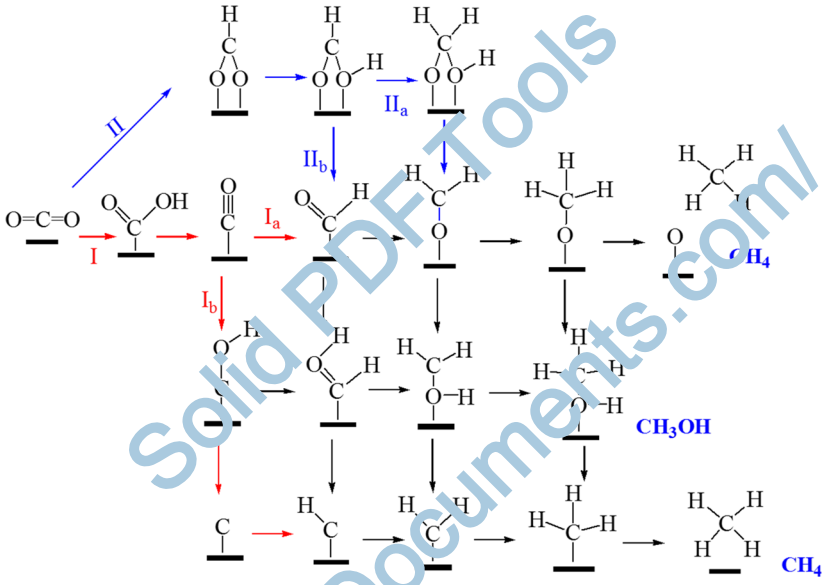

[a]The (H^+ + e^-) reactant and H_2O product are left out for brevity.

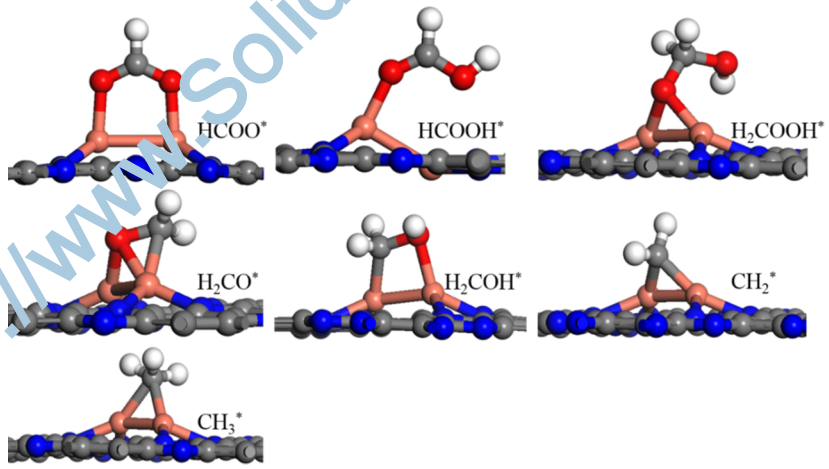

Figure 2. Optimized geometric structures of various states (HCOO*, HCOOH*, H_2COOH*, H_2CO*, H_2COH*, CH_2*, and CH_3*) along the most favorable reaction path of the CO_2RR proceeded on a $Cu_2@C_2N$ monolayer.

DOI: 10.1021/acs.jpcc.8b06494
J. Phys. Chem. C 2018, 122, 19712−19721

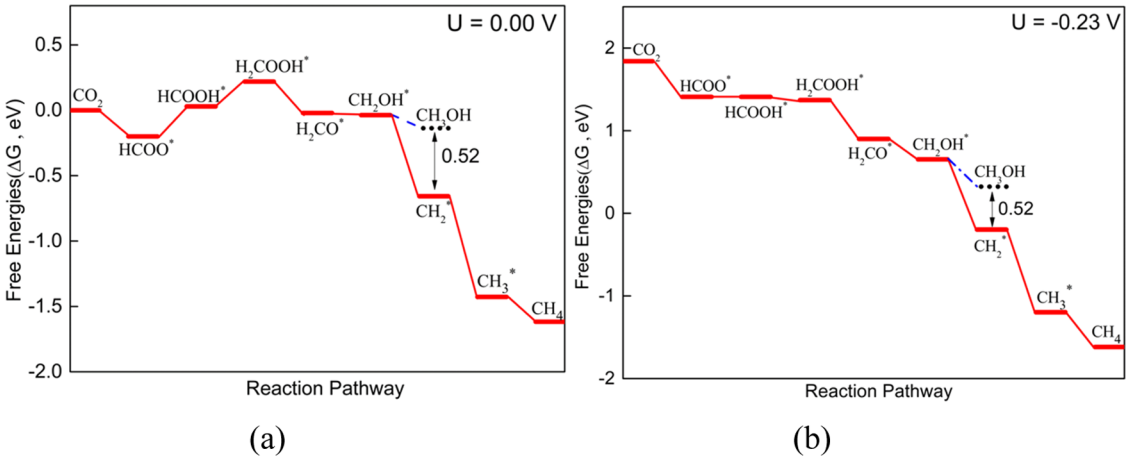

Figure 3. Free energy profile for the CO_2RR to CH_3OH and CH_4 on $Cu_2@C_2N$ at (a) 0.00 V and (b) −0.23 V.

change in zero-point energies, and $T\Delta S$ is the entropy change at room temperature (T = 298.15 K), ΔG_U is the contribution of electrode potential (U) to ΔG. The zero-point energies and entropies of the CO_2RR species were computed from the vibrational frequencies, in which only the adsorbate vibrational modes were computed explicitly, while the catalyst was fixed. The entropies of the free molecules gas-phase molecules were obtained from the standard thermodynamic database. To simulate the real H_2O solvent environment, a conductor-like screening model was used, in which the dielectric constant was set as 78.54 for H_2O solvent.[66]

3. RESULTS AND DISCUSSION

3.1. Structures and Stability of $Cu_2@C_2N$. We first examined the structures and stability of the Cu dimer

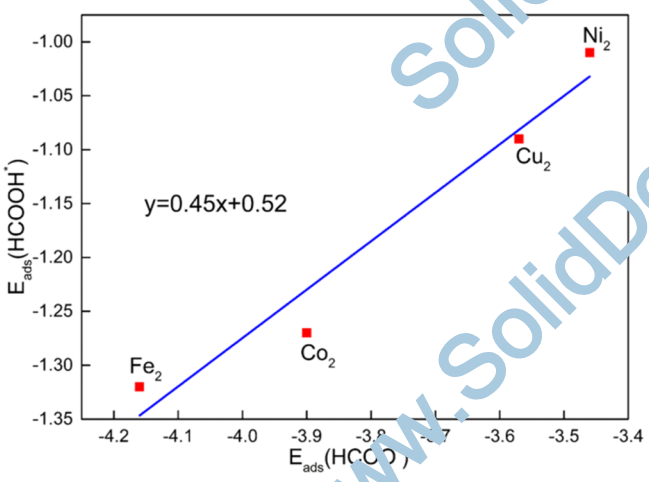

Figure 4. Correlation between E_{ads}(HCOO*) and E_{ads}(HCOOH*) for $TM_2@C_2N$.

supported on a C_2N layer, and two initial structures were considered, in which the two Cu atoms are located on the same side (labeled as Con-1) and different sides (labeled as Con-2) of the C_2N surface, respectively. After full atomic relaxations, however, we found that Con-1 is not stable as it would be optimized to Con-2, which is well consistent with previous theoretical report.[54] As shown in Figure 1a, each Cu atom in $Cu_2@C_2N$ interacts strongly with two N atoms with the bond length of 1.99 Å and the Cu−Cu bond length is 2.35 Å.

To evaluate the structural stability of a Cu dimer on a C_2N layer, we computed the corresponding adsorption energy. The computed adsorption energy (−3.58 eV) is larger than the Cu bulk cohesive energy (−3.38 eV), indicating the high stability and experimental feasibility for the anchoring of Cu on a porous C_2N layer. Meanwhile, the local charge density of $Cu_2@C_2N$ mainly localizes on the Cu dimer (+0.62 e^-), while the Cu-bonded N atoms (−0.19 e^-) are slightly polarized. In general, adsorption sites with large charges typically have strong interactions with reaction intermediates. Thus, the anchored Cu bi-atoms are expected to be the active sites for CO_2RR.

The electronic structures can provide a good description of electron distributions in molecules and solids, which are useful tools for chemical bond classification. Thus, we computed the band structure and partial density of states (PDOS) of $Cu_2@C_2N$ (Figure 1), and in particular examined its band gap and charge distribution in the bands near the Fermi level, since these bands are active in the CO_2RR and will interact with reaction intermediates. Our computed band gap of a pristine C_2N layer is 1.77 eV. A $Cu_2@C_2N$ layer does not contain any magnetic moment. Because the occupied d bands of the Cu atoms lie in the gap of the band structures of C_2N, the band gap of a $Cu_2@C_2N$ layer is greatly reduced to 0.58 eV, suggesting an improved electroconductivity. Furthermore, the computed PDOS suggested strong hybridization between Cu 3d and N 2p orbitals, further testifying the strong interaction of a Cu dimer with the C_2N layer.

3.2. CO_2 Electrocatalytic Reduction. After examining the geometric structures, stabilities, and electronic structures of the Cu dimer supported on a porous C_2N layer, we investigated the CO_2RR catalytic activity on $Cu_2@C_2N$. Two possible pathways, namely the C_1 and C_2 pathways, have been considered. Special attention was given to identify the kinetically most favorable reaction routes (the lowest-energy pathway) on $Cu_2@C_2N$, which has the lowest positive elementary free energy change between any two elementary steps, and to determine the thermodynamic limiting potential, the least-negative potential at which all of the elementary steps become exergonic (downhill in free energy).

3.2.1. C_1 Pathway. We first studied the C_1 pathway and considered different possible channels (Scheme 1), in which various C1 products, such as CH_4, CO, HCOOH, and

DOI: 10.1021/acs.jpcc.8b06494
J. Phys. Chem. C 2018, 122, 19712−19721

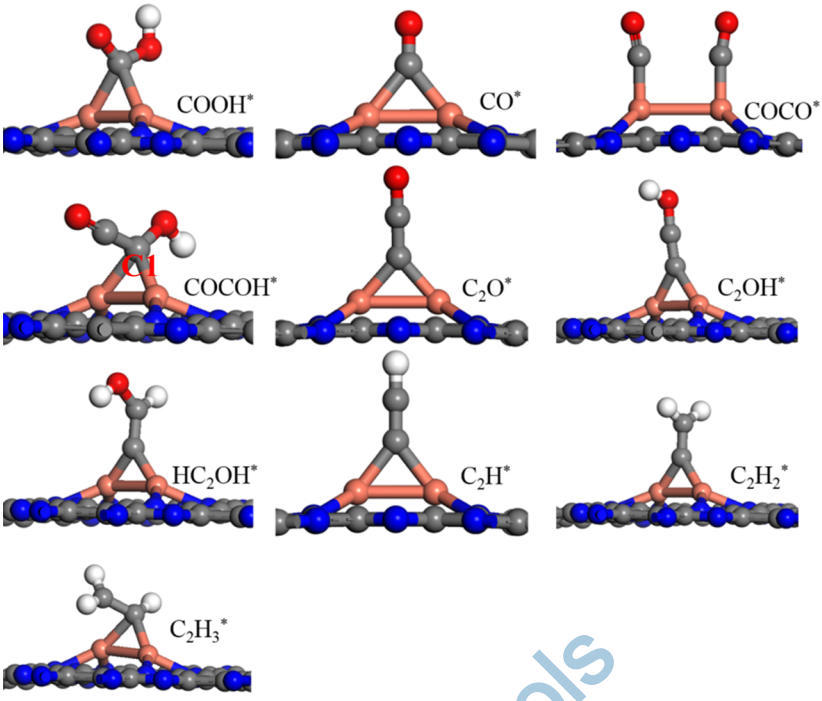

Figure 5. Optimized geometric structures of various states (COOH*, CO*, CO[illegible], COCOH*, C_2O*, C_2OH*, HC_2OH*, C_2H*, C_2H_3*, and C_2H_3*) along the most favorable C_2 pathway in the CO_2RR proceeded on [illegible] $Cu_2@C_2N$ monolayer.

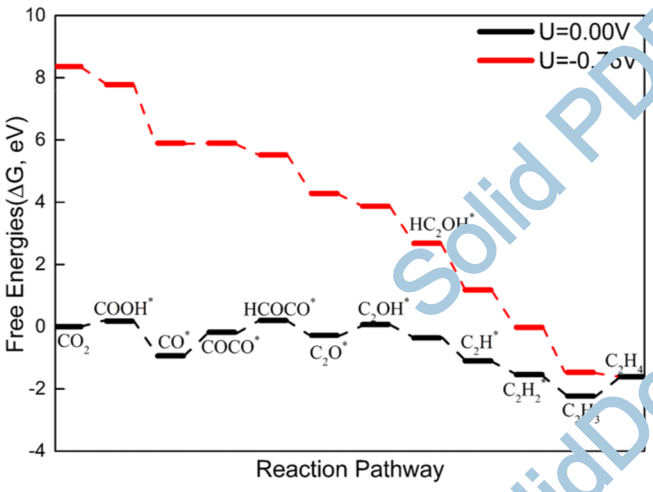

Figure 6. Free energy profile for the CO_2RR to C_2H_4 on [illegible] $@C_2N$ at 0.00 and −0.76 V.

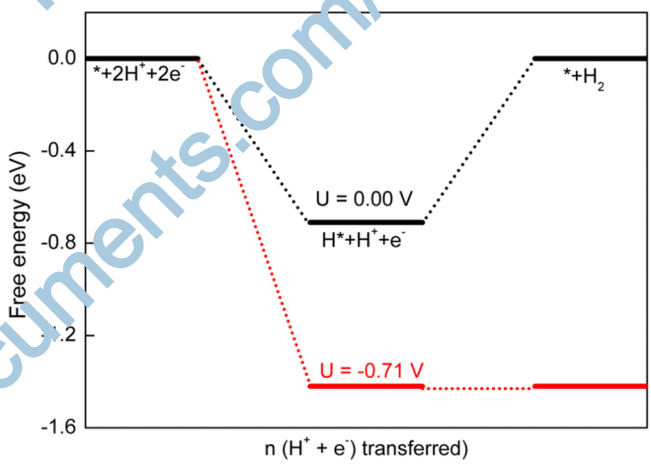

Figure 7. Free energy profile for the HER on $Cu_2@C_2N$ at 0 and −0.71 V.

CH_3OH, could be formed.[67] For brevity, the proton−electron couple ($H^+ + e^-$) was omitted. Figure 2 displays the atomic configurations at various states along the lowest-energy pathway, and the key structural parameters are summarized in Table S1. In addition, the corresponding free energy profiles are presented in Figure 3.

As shown in Scheme 1, the CO_2RR starts by the hydrogenation of CO_2 to form either adsorbed carboxyl (COOH*, path I) or formate (HCOO*, path II) on the catalyst, which is crucial to determine or influence the entire reaction pathways. It is well established that the hydrogenation of COOH* species will produce CO*, which can then either release from the catalyst surface (CO* → * + CO) or be further protonated to CHO* (path Ia)/COH* (path 1b) (CO* + H^+ + e^- → CHO*/COH*). Once the CO_2RR proceeds along the HCOO* pathway, the adsorbed HCOO* species can be hydrogenated to HCOOH*, which could be further hydrogenated (path IIa) or desorb off from the catalyst surface (path IIb).

For the COOH* species on $Cu_2@C_2N$, we found that it prefers to adsorb on the Cu−Cu bridge site, resulting in the formation of two C−Cu bonds with the bond length of 2.03 Å. On the contrary, the HCOO* species prefers to adopt a bidentate adsorption mode, forming two O−Cu bonds with the distance of 1.94 Å (Figure 2). Meanwhile, the adsorption of COOH* and HCOO* species pulls the two Cu atoms out the C_2N plane. Remarkably, the HCOO* formation is exothermic in the free energy profile by 0.20 eV (Figure 2), while the COOH* formation is endothermic by 0.18 eV, suggesting that energetically the formation of HCOO* is more favorable than that of COOH*.

Providing that the CO_2RR proceeds along the path I, the COOH* species can be hydrogenated to form CO* species by

DOI: 10.1021/acs.jpcc.8b06494
J. Phys. Chem. C 2018, 122, 19712−19721

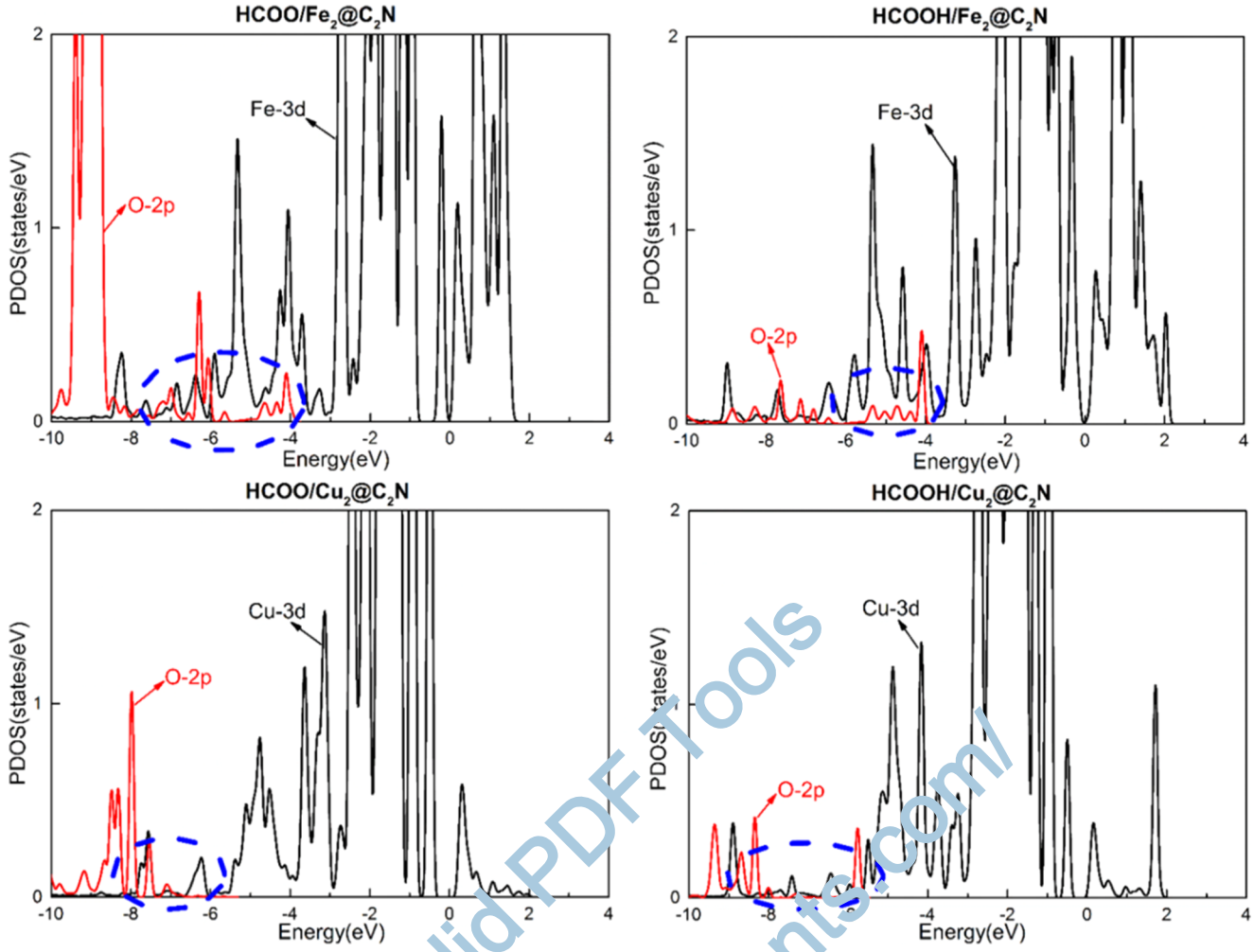

Figure 8. Projected density of states (PDOS) of the $Fe_2@C_2N$ and $Cu_2@C_2N$ with adsorbed HCOO and HCOOH species. The Fermi level is referenced at 0 eV.

reacting with a proton coupled with an electron transfer. Remarkably, this reaction, that is, COOH* + H^+ + e^- → CO* + H_2O(g), is exothermic in the free energy profile by 1.12 eV. Following the production of CO, the next key step is the hydrogenation of the adsorbed CO to form either adsorbed CHO* (path Ia) or COH* (path Ib). However, these two processes are uphill in the free energy profile by 1.16 and 1.44 eV, respectively, suggesting that the further hydrogenation of the adsorbed CO species to CHO* or COH* is energetically unfavorable on $Cu_2@C_2N$. Thus, the following hydrogenation of CHO* or COH* species was not considered. In addition to the formation CHO* and COH* species, the adsorbed CO* could couple with another CO to generate C2 products, which will be discussed in Section 3.2.2.

On the other hand, once the HCOO* species is formed along path II, it can be further hydrogenated to form various products. Thus, we carefully investigated these hydrogenation steps to determine the lowest-energy pathway and the product selectivity. On the basis of the computed free energies of each elementary step at zero potential (Figure 3a), our results revealed that the CO_2 → HCOO* → HCOOH* → H_2COOH* → H_2CO* → H_2COH* → CH_2* → CH_3* → CH_4 path is the most favorable path from a purely thermodynamic perspective. Note that there is also a thermodynamically less favorable pathway from H_2COH*, leading to the CH_3OH formation (H_2COH* → CH_3OH). During the whole 8e transfer process, the hydrogenation of HCOO* to HCOOH* is the potential-determining step (PDS), since this step has the most positive free energy change (ΔG = +0.23 eV), and the limiting potential of the whole process is −0.23 eV (Figure 3b). Such a preferable reaction pathway and the PDS are different from those on Cu(111) surface[67] or Cu_{55} nanoparticles supported defective graphene,[68] in which a gas-phase CO_2 molecule is reduced to CH_4 via the following pathway: CO_2 → COOH* → CO* → CHO* → CH_2O* → CH_3O* → CH_4, and the formation of CHO* species is the PDS. The difference between $Cu_2@C_2N$ and Cu_{55}/graphene may be ascribed to the stronger adsorption on $Cu_2@C_2N$ (−2.01 eV), which makes the free energy barrier required to surmount this step (1.16 eV) much higher than that on Cu_{55}/graphene (0.68 eV).[68]

According to our above discussions, the computed overpotential for CH_4 production on $Cu_2@C_2N$ is −0.23 V, which is much lower than that on Cu(111) surface (−0.97 V)[67] and the graphene-supported Cu_{55} cluster (−0.68 V).[68] The obvious decrease in the free energy barrier results in an about 0.45−0.74 V reduction in the applied potential, making the whole reaction step exothermic, in other words, smaller overpotential and less power consumption. Therefore, $Cu_2@C_2N$ exhibits

DOI: 10.1021/acs.jpcc.8b06494
J. Phys. Chem. C 2018, 122, 19712−19721

much higher catalytic activity for the CO_2RR than the Cu_{55}/graphene or Cu(111) surface.

Another interesting question is the product distribution, that is, CH_4 vs CH_3OH, which is greatly dependent on the adsorption energy of O on catalyst surfaces. On $Cu_2@C_2N$ surface, the significantly strong O adsorption ($E_{ads} = -1.86$ eV, evaluated by using half of the O_2 molecule as a reference) makes it more difficult for Cu−O bond dissociation (leading to CH_3OH formation), as compared with the C−O bond breakage (leading to CH_4 formation). Therefore, CH_4 production is ∼0.52 eV more favorable than that of CH_3OH (Figure 3). To estimate the distribution of CH_4 vs CH_3OH, the Boltzmann distribution formula $\exp[-(\Delta G)/(k_B T)]$ can be utilized according to the computed free energy difference, where ΔG is −0.52 eV and T is 298.15 K. Thus, the CH_4/CH_3OH molecular ratio is $\sim(6.2 \times 10^8)$:1 at ambient temperature, suggesting a high selectivity of $Cu_2@C_2N$ toward CH_4 production.

Note that the Ni, Fe, or Co atoms supported on N-doped carbon nanostructures have been widely used as nonprecious electrocatalysts for the CO_2RR.[69−71] For example, Li et al. demonstrated that the Ni−N_4−C structure exhibits excellent activity for electrochemical reduction of CO_2 with particularly high selectivity and high faradaic efficiency (over 90%) for CO production.[69] Zhang et al. synthesized atomic iron dispersed on nitrogen-doped graphene as an efficient electrocatalyst for CO_2 reduction to CO, which has a low reduction overpotential with high faradaic efficiency up to 80%.[70] Pan et al. demonstrated that single-atom Co−N_5 site anchored on polymer-derived hollow N-doped porous carbon spheres exhibits a robust electrocatalytic activity for CO_2 reduction with nearly 100% CO selectivity.[71] Then, the following interesting questions arise naturally: Can the Fe, Co, and Ni dimers on a C_2N layer (Figure S1) be used as CO_2RR? If yes, as compared with $Cu_2@C_2N$, will these three dimers exhibit similar catalytic activity for the CO_2RR?

To answer these questions, we computed the CO_2RR pathways on Fe, Co, and Ni dimers supported on a C_2N layer, in which we determined only the free energy of the hydrogenation of HCOO* to HCOOH* since it is the potential-determining step on $Cu_2@C_2N$. Our computations showed that the free energies of the above step are 0.81, 0.50 and 0.34 eV, respectively, on these three catalysts, which are all larger than that on $Cu_2@C_2N$ (0.23 eV). Thus, we predicted that a C_2N-supported Cu dimer exhibits higher CO_2RR catalytic activity than Fe, Co, and Ni dimers supported on a C_2N layer.

To gain deeper insight into the difference of the CO_2RR catalytic activity on Fe, Co, Ni, and Cu dimers, we computed their adsorption strengths with HCOO* and HCOOH* species that are two important intermediates in the PDS. A good correlation exists between the adsorption energies of these two intermediates on our TM dimers (Figure 4). Remarkably, $Cu_2@C_2N$ exhibits a relatively moderate binding ability to HCOO* ($E_{ads} = -3.57$ eV) and HCOOH* (−1.09 eV), relatively weaker than those on $Fe_2@C_2N$ (−4.17 and −1.32 eV) and $Co_2@C_2N$ (−3.90 and −1.27 eV) but stronger than those on $Ni_2@C_2N$ (−3.16 and −0.79 eV, respectively, for HCOO* and HCOOH*). According to the Sabatier principle, $Cu_2@C_2N$ with a moderate adsorption strength with HCOO* and HCOOH* should have higher CO_2RR catalytic activity than other three $TM_2@C_2N$, which is well consistent with their limiting potentials for the CO_2RR (−0.81, −0.50, −0.34, and −0.23 V on Fe, Co, Ni, and Cu dimers supported by C_2N).

To what extent does the bi-atom catalyst $Cu_2@C_2N$ improve the CO_2RR catalytic performance with respect to the single-atom catalyst? To address this question, we investigated the single-atom catalyst, $Cu@C_2N$, in which an individual Cu atom is adsorbed on a C_2N layer. However, checking the first few steps of CO_2 electroreductions on $Cu@C_2N$ can already eliminate it as a good catalyst: the free energy changes for the formation of COOH* and HCOO* are 1.18 and 0.83 eV, respectively (Figure S2), which are much larger than the maximum free energy change of the CO_2RR on Cu dimer (0.23 eV). Obviously, the bi-atom catalyst $Cu_2@C_2N$ has much better catalytic performance for the CO_2RR than its single-atom counterpart.

3.2.2. C_2 Pathway. Previous theoretical studies showed that the C_2 hydrocarbon species could be generated on Cu-based catalysts, which generally begins from the CO* dimerization.[72,73] Can C_2 species be generated on $Cu_2@C_2N$? To address this question, we examined C_2 species formation pathway.

Figure 5 presents the atomic configurations at various states along the C_2 pathway, and the corresponding free energy profiles are summarized in Figure 6. Our results demonstrated that the C atom in the CO* species, which can be yielded from the COOH* hydrogenation, has formal three-coordination (Figure 5), making it highly active to couple with another CO molecule to form COCO* species. In the formed COCO* species (Figure 5), the two CO species are separately adsorbed on the Cu sites with the Cu−C bond length of 1.81 Å and the C−C distance between two CO species is 2.79 Å. Remarkably, at zero potential, this reaction from (CO* + CO) → COCO* is uphill by 0.7[illegible] eV in the free energy profile (Figure 6), which is lower than that of CO* hydrogenation to CHO* (1.16 eV) or COH* (1.44 eV).

Subsequently, the hydrogenation of O atoms in COCO* species could produce COCOH* species, in which one C atom (denoted as C1) is adsorbed on the Cu−Cu bridge, while the other C atom binds with C1 atom with the length of 1.34 Å, suggesting the formation of a stable C−C bond. The approach of a second hydrogen induces the dissociation of COCOH* species into C_2O* and H_2O. The C_2O* would be further hydrogenated to the final product C_2H_4 by six hydrogenation steps. During the whole C_2 pathway, the formation of COCO* species is the PDS because of its maximum positive free energy change (0.76 eV), suggesting the high catalytic activity of $Cu_2@C_2N$ for the CO_2RR to C_2H_4.

3.2.3. Side Reaction Analyses. In addition to CH_4 and C_2H_4 production, the occurring CO_2RR in an aqueous solution would compete with the hydrogen evolution reaction (HER) because H* can also adsorb on the catalysts under the same reaction conditions by consuming the same proton−electron pair ($H^+ + e^-$).[74] Clearly, the HER greatly affects the faradaic efficiency at low pH region. Thus, an effective CO_2RR catalyst should exhibit poor activity for the competitive HER.[75,76]

To examine the effect of the HER on the CO_2RR, we studied the free energy changes (ΔG) of the HER on $Cu_2@C_2N$. Our results showed that a free energy barrier of 0.71 eV is required in the H_2 gas desorption step ($H^* + H \rightarrow H_2$) (Figure 7), which is larger than that of CH_4 production in the CO_2RR (0.23 eV) and is only slightly lower than that of C_2H_4 generation (0.76 eV). Notably, compared to the free energy barrier of the HER on a typical metal electrode (0.05−0.15

DOI: 10.1021/acs.jpcc.8b06494
J. Phys. Chem. C 2018, 122, 19712−19721

meV),[77] the free energy barrier of the HER on $Cu_2@C_2N$ is rather high. Considering that adjusting the electrolyte pH and adopting nonaqueous solutions are capable of effectively suppressing the HER,[78] it is possible to minimize the influence of this side reaction on the CO_2RR under real experimental adjustments.

3.2.4. Electronic Structures Analyses. On the basis of the aforementioned analyses, it is clear that the Cu_2 dimer supported on a C_2N layer exhibits high catalytic activity for the CO_2RR because of its moderate interaction with the CO_2RR species. To deeply understand the remarkable difference in the CO_2RR catalytic activity among different $TM_2@C_2N$, we investigated the electronic structures of $TM_2@C_2N$.

Figure 8 shows the calculated partial density of states (PDOS) of two key CO_2RR intermediates, that is, HCOO* and HCOOH*, on the deposited TM dimers on C_2N surface, where the Cu and Fe dimers were chosen as the representative, since the Cu dimer shows the lowest limiting (−0.23 V) and the Fe dimer has the highest limiting potential (−0.81 V) for CH_4 production. To facilitate their comparison, the PDOS were plotted for the same energy window from −10 to 4 eV.

Our results show that on $Fe_2@C_2N$, the 2p states of the adsorbed HCOO* species are delocalized and have a strong hybridization with Fe 3d states in a rather broad energy range from −8.54 to −3.78 eV. In contrast, the $Cu_2@C_2N$ layer and HCOO* have much weaker hybridization in a limited range between −8.13 and −7.33 eV. The similar phenomenon was also found in the case of the HCOOH* adsorption on $Cu_2@C_2N$ and $Fe_2@C_2N$ surfaces (Figure 8). The much-pronounced hybridization on $Fe_2@C_2N$ indicates that its interaction with the CO_2RR species is too strong, resulting in a higher limiting potential.

4. CONCLUSIONS

In summary, by means of DFT simulations, we studied the possible pathways for electrochemical reduction of CO_2 on several TM dimers supported on C_2N. Our results showed that $Cu_2@C_2N$ exhibits a moderate adsorption ability to CO_2RR species intermediates, endowing its higher catalytic performance for the reduction of CO_2. Remarkably, $Cu_2@C_2N$ has a high selective generation of CH_4 rather than CH_3OH, in which the hydrogenation of HCOO* to HCOOH* is identified as the potential-determining step with the limiting potential of −0.23 V. In addition, the effective coupling between CO species leads to the generation of C_2H_4. These findings not only offer theoretical insights into the reduction pathways of CO_2RR, but also open a new avenue to design metal-dimer-based and related bi-atom electrocatalysts for CO_2 electroreduction. Note that the cooperative effects of the metal dimer in the bi-atom catalysts may greatly improve the activity and selectivity of a catalytic reaction. Further studies on the deposition of different metal dopant pairs or alloys on porous nanomaterials would lead to even better improvement of the CO_2RR activity.

■ ASSOCIATED CONTENT

Supporting Information

The Supporting Information is available free of charge on the ACS Publications website at DOI: 10.1021/acs.jpcc.8b06494.

Some key structural parameters, optimized structures of other $TM_2@C_2N$, and the free energy profiles of the first few steps of the CO_2RR on $Cu@C_2N$ and the involved intermediates (PDF)

■ AUTHOR INFORMATION

Corresponding Authors

*E-mail: xjz_hmily@163.com (J.Z.).
*E-mail: zhongfangchen@gmail.com (Z.C.).

ORCID

Jingxiang Zhao: 0000-0001-6023-8887
Zhongfang Chen: 0000-0002-1445-9184

Notes

The authors declare no competing financial interest.

■ ACKNOWLEDGMENTS

This work was financially supported in China by the Natural Science Funds for Distinguished Young Scholar of Heilongjiang Province (No. JC2018004), the Excellent Young Foundation of Harbin Normal University (Grant No. XKYQ201304), and National Natural Science Foundation of China (No. 11704203), and in United States by NSF-CREST Center for Innovation, Research and Education in Environmental Nanotechnology (CIRE2N) (Grant Number HRD-1736098).

■ REFERENCES

(1) Olah, G. A.; Prakash, G. K. S.; Goeppert, A. Anthropogenic Chemical Carbon Cycle for a Sustainable Future. *J. Am. Chem. Soc.* **2011**, *133*, 12881−12898.

(2) Jhong, H.-R. M.; Ma, S.; Kenis, P. J. A. Electrochemical Conversion of CO_2 to Useful Chemicals: Current Status, Remaining Challenges, and Future Opportunities. *Curr. Opin. Chem. Eng.* **2013**, *2*, 191−199.

(3) Costentin, C.; Robert, M.; Saveant, J.-M. Catalysis of the Electrochemical Reduction of Carbon Dioxide. *Chem. Soc. Rev.* **2013**, *42*, 2423−2436.

(4) Wang, W.; Wang, S.; Ma, X.; Gong, J. Recent Advances in Catalytic Hydrogenation of Carbon Dioxide. *Chem. Soc. Rev.* **2011**, *40*, 3703−3727.

(5) Qiao, J.; Liu, Y.; Hong, F.; Zhang, J. A Review of Catalysts for the Electroreduction of Carbon Dioxide to Produce Low-Carbon Fuels. *Chem. Soc. Rev.* **2014**, *43*, 631−675.

(6) Zhu, D. D.; Liu, J. L.; Qiao, S. Z. Recent Advances in Inorganic Heterogeneous Electrocatalysts for Reduction of Carbon Dioxide. *Adv. Mater.* **2016**, *28*, 3423−3452.

(7) Benson, E. E.; Kubiak, C. P.; Sathrum, A. J.; Smieja, J. M. Electrocatalytic and Homogeneous Approaches to Conversion of CO_2 to Liquid Fuels. *Chem. Soc. Rev.* **2009**, *38*, 89−99.

(8) Kuhl, K. P.; Hatsukade, T.; Cave, E. R.; Abram, D. N.; Kibsgaard, J.; Jaramillo, T. F. Electrocatalytic Conversion of Carbon Dioxide to Methane and Methanol on Transition Metal Surfaces. *J. Am. Chem. Soc.* **2014**, *136*, 14107−14113.

(9) Hori, Y.; Murata, A.; Takahashi, R. Formation of Hydrocarbons in the Electrochemical Reduction of Carbon Dioxide at a Copper Electrode in Aqueous Solution. *J. Chem. Soc., Faraday Trans. 1* **1989**, *85*, 2309−2326.

(10) Nie, X.; Esopi, M. R.; Janik, M. J.; Asthagiri, A. Selectivity of CO_2 Reduction on Copper Electrodes: the Role of the Kinetics of Elementary Steps. *Angew. Chem., Int. Ed.* **2013**, *52*, 2459−2462.

(11) Schouten, K. J. P.; Kwon, Y.; van der Ham, C. J. M.; Qin, Z.; Koper, M. T. M. A New Mechanism for the Selectivity to C1 And C2 Species in the Electrochemical Reduction of Carbon Dioxide on Copper Electrodes. *Chem. Sci.* **2011**, *2*, 1902−1909.

(12) Zhang, B.; Zhang, J. Rational Design of Cu-Based Electrocatalysts for Electrochemical Reduction of Carbon Dioxide. *J. Energy Chem.* **2017**, *26*, 1050−1066.

DOI: 10.1021/acs.jpcc.8b06494
J. Phys. Chem. C 2018, 122, 19712−19721

(13) Lee, C. W.; Dong, Y. K.; Dae-Hyun, N.; Ho, J. J.; Heon, C. N.; Won, I. S.; Tae, N. K. Defining a Materials Database for the Design of Copper Binary Alloy Catalysts for Electrochemical CO_2 Conversion. *Adv. Mater.* **2018**, No. 1704717.
(14) Raciti, D.; Livi, K. J.; Wang, C. Highly Dense Cu Nanowires for Low-Overpotential CO_2 Reduction. *Nano Lett.* **2015**, *15*, 6829−6835.
(15) Huang, P.; Ci, S.; Wang, G.; Jia, J.; Xu, J.; Wen, Z. High-Activity Cu Nanowires Electrocatalysts for CO_2 Reduction. *J. CO_2 Util.* **2017**, *20*, 27−33.
(16) Cao, L.; Raciti, D.; Li, C.; Livi, K. J. T.; Rottmann, P. F.; Hemker, K. J.; Mueller, T.; Wang, C. Mechanistic Insights for Low-Overpotential Electroreduction of CO_2 to CO on Copper Nanowires. *ACS Catal.* **2017**, *7*, 8578−8587.
(17) Raciti, D.; Cao, L.; Livi, K. J. T.; Rottmann, P. F.; Tang, X.; Li, C.; Hicks, Z.; Bowen, K. H.; Hemker, K. J.; Mueller, T.; Wang, C. Low-Overpotential Electroreduction of Carbon Monoxide Using Copper Nanowires. *ACS Catal.* **2017**, *7*, 4467−4472.
(18) Mandal, L.; Yang, K. R.; Motapothula, M. R.; Ren, D.; Lobaccaro, P.; Patra, A.; Sherburne, M.; Batista, V. S.; Yeo, B. S.; Ager, J. W.; et al. Investigating the Role of Copper Oxide in Electrochemical CO_2 Reduction in Real Time. *ACS Appl. Mater. Interfaces* **2018**, *10*, 8574−8584.
(19) Lum, Y.; Yue, B.; Lobaccaro, P.; Bell, A. T.; Ager, J. W. Optimizing C−C Coupling on Oxide-Derived Copper Catalysts for Electrochemical CO_2 Reduction. *J. Phys. Chem. C* **2017**, *121*, 14191−14203.
(20) Verdaguer-Casadevall, A.; Li, C. W.; Johansson, T. P.; Scott, S. B.; McKeown, J. T.; Kumar, M.; Stephens, I. E. L.; Kanan, M. W.; Chorkendorff, I. Probing the Active Surface Sites for CO Reduction on Oxide-Derived Copper Electrocatalysts. *J. Am. Chem. Soc.* **2015**, *137*, 9808−9811.
(21) Shinagawa, T.; Larrazábal, G. O.; Martín, A. J.; Krumeich, F.; Pérez-Ramírez, J. Sulfur-Modified Copper Catalysts for the Electrochemical Reduction of Carbon Dioxide to Formate. *ACS Catal.* **2018**, *8*, 837−844.
(22) Zhao, Z.; Peng, X.; Liu, X.; Sun, X.; Shi, J.; Han, L.; Li, G.; Luo, J. Efficient and Stable Electroreduction of CO_2 to CH_4 on CuS nanosheet arrays. *J. Mater. Chem. A* **2017**, *5*, 20239−20243.
(23) Hossain, M. N.; Wen, J.; Chen, A. Innate Copper and Reduced Graphene Oxide Nanocomposite toward the Efficient Electrochemical Reduction of Carbon Dioxide. *Sci. Rep.* **2017**, *7*, No. 3184.
(24) Baturina, O. A.; Lu, Q.; Padilla, M. A.; Xin, L.; Li, W.; Serov, A.; Artyushkova, K.; Atanassov, P.; Xu, F.; Epshteyn, A.; et al. CO_2 Electroreduction to Hydrocarbons on Carbon-Supported Cu Nanoparticles. *ACS Catal.* **2014**, *4*, 3682−3695.
(25) Yang, W.; Dastafkan, K.; Jia, C.; Zhao, C. Design of Electrocatalysts and Electrochemical Cells for Carbon Dioxide Reduction Reactions. *Adv. Mater. Technol.* **2018**, No. 1700177.
(26) Yang, X.-F.; Wang, A.; Qiao, B.; Li, J.; Liu, J.; Zhang, T. Single-Atom Catalysts: A New Frontier in Heterogeneous Catalysis. *Acc. Chem. Res.* **2013**, *46*, 1740−1748.
(27) Liang, S.; Hao, C.; Shi, Y. The Power of Single-Atom Catalysis. *ChemCatChem* **2015**, *7*, 2559−2567.
(28) Qiao, B.; Wang, A.; Yang, X.; Allard, L. F.; Jiang, Z.; Cui, Y.; Liu, J.; Li, J.; Zhang, T. Single-Atom Catalysis of CO Oxidation Using Pt_1/FeO_x. *Nat. Chem.* **2011**, *3*, 634.
(29) Bayatsarmadi, B.; Zheng, Y.; Vasileff, A.; Qiao, S. Z. Recent Advances in Atomic Metal Doping of Carbon-based Nanomaterials for Energy Conversion. *Small* **2017**, *13*, No. 1700191.
(30) Liu, J. Catalysis by Supported Single Metal Atoms. *ACS Catal.* **2017**, *7*, 34−59.
(31) Li, Z.; Wang, D.; Wu, Y.; Li, Y. Recent Advances in the Precise Control of Isolated Single Site Catalysts by Chemical Methods. *Natl. Sci. Rev.* **2018**, No. nwy056.
(32) Wang, L.; Zhang, S.; Zhu, Y.; Patlolla, A.; Shan, J.; Yoshida, H.; Takeda, S.; Frenkel, A. I.; Tao, F. Catalysis and In Situ Studies of Rh_1/Co_3O_4 Nanorods in Reduction of NO with H_2. *ACS Catal.* **2013**, *3*, 1011−1019.
(33) Qiao, B.; Liu, J.; Wang, Y.-G.; Lin, Q.; Liu, X.; Wang, A.; Li, J.; Zhang, T.; Liu, J. Highly Efficient Catalysis of Preferential Oxidation of CO in H_2-Rich Stream by Gold Single-Atom Catalysts. *ACS Catal.* **2015**, *5*, 6249−6254.
(34) Huang, Z.; Gu, X.; Cao, Q.; Hu, P.; Hao, J.; Li, J.; Tang, X. Catalytically Active Single-Atom Sites Fabricated from Silver Particles. *Angew. Chem., Int. Ed.* **2012**, *51*, 4198−4203.
(35) Li, F.; Li, Y.; Zeng, X. C.; Chen, Z. Exploration of High-Performance Single-Atom Catalysts on Support M_1/FeO_x for CO Oxidation via Computational Study. *ACS Catal.* **2015**, *5*, 544−552.
(36) Liang, J.-X.; Yang, X.-F.; Wang, A.; Zhang, T.; Li, J. Theoretical Investigations of Non-Noble Metal Single-Atom Catalysis: Ni_1/FeO_x for CO oxidation. *Catal. Sci. Technol.* **2016**, *6*, 6886−6892.
(37) Long, B.; Tang, Y.; Li, J. New Mechanistic Pathways for CO Oxidation Catalyzed by Single-Atom Catalysts: Supported and Doped Au_1/ThO_2. *Nano Res.* **2016**, *9*, 3868−3880.
(38) Yang, T.; Ryoichi, F.; Saburo, H.; Tsunehiro, T.; Shigeyoshi, S.; Masahiro, E. A Theoretical Investigation on CO Oxidation by Single-Atom Catalysts M_1/γ-Al_2O_3 (M = Pd, Fe, Co, and Ni). *ChemCatChem* **2017**, *9*, 1222−1229.
(39) Zhu, C.; Fu, S.; Shi, Q.; Du, D.; Lin, Y. Single-Atom Electrocatalysts. *Angew. Chem., Int. Ed.* **2017**, *56*, 13944−13960.
(40) Liu, C.; Yang, B.; Tyo, E.; Seifert, S.; DeBartolo, J.; von Issendorff, B.; Zapol, P.; Vajda, S.; Curtiss, L. A. Carbon Dioxide Conversion to Ethanol over Size-Selected Cu_4 Clusters at Low Pressures. *J. Am. Chem. Soc.* **2015**, *137*, 8676−8679.
(41) Liu, J.-C.; Ma, X.-L.; Li, Y.; Wang, Y.-G.; Xiao, H.; Li, J. Heterogeneous Fe_3 Single-Cluster Catalyst for Ammonia Synthesis via an Associative Mechanism. *Nat. Commun.* **2018**, *9*, No. 1610.
(42) Matsushita, O.; Derkacheva, V. M.; Muranaka, A.; Shimizu, S.; Uchiyama, M.; Luk'yanets, E. A.; Kobayashi, N. Rectangular-Shaped Expanded Phthalocyanines with Two Central Metal Atoms. *J. Am. Chem. Soc.* **2012**, *134*, 3411−3418.
(43) He, Z.; He, K.; Robertson, A. W.; Kirkland, A. I.; Kim, D.; Ihm, J.; Yoon, E.; Lee, G. D.; Warner, J. H. Atomic Structure and Dynamics of Metal Dopant Pairs in Graphene. *Nano Lett.* **2014**, *14*, 3766−3772.
(44) Yan, H.; Lin, Y.; Wu, H.; Zhang, W.; Sun, Z.; Cheng, H.; Liu, W.; Wang, C.; Li, J.; Huang, X.; Yao, T.; et al. Bottom-Up Precise Synthesis of Stable Platinum Dimers on Graphene. *Nat. Commun.* **2017**, *8*, No. 1070.
(45) Xian, S.; Fu, Q.; Chen, W.; Feng, Q.; Chen, Z.; Zhang, J.; Cheong, W.-C.; Yu, R.; Gu, L.; Dong, J.; et al. Carbon Nitride Supported Fe_2 Cluster Catalysts with Superior Performance for Alkene Epoxidation. *Nat. Commun.* **2018**, *9*, No. 2353.
(46) Zhu, G.; Li, Y.; Zhu, H.; Su, H.; Chan, S. H.; Sun, Q. Enhanced CO_2 Electroreduction on Armchair Graphene Nanoribbons Edge-Decorated with Copper. *Nano Res.* **2017**, *10*, 1641−1650.
(47) Li, Y.; Su, H.; Chan, S. H.; Sun, Q. CO_2 Electroreduction Performance of Transition Metal Dimers Supported on Graphene: A Theoretical Study. *ACS Catal.* **2015**, *5*, 6658−6664.
(48) Shen, H.; Li, Y.; Sun, Q. CO_2 Electroreduction Performance of Phthalocyanine Sheet with Mn Dimer: a Theoretical Study. *J. Phys. Chem. C* **2017**, *121*, 3963−3969.
(49) Mahmood, J.; Lee, E. K.; Jung, M.; Shin, D.; Jeon, I.-Y.; Jung, S.-M.; Choi, H.-J.; Seo, J.-M.; Bae, S.-Y.; Sohn, S.-D.; et al. Nitrogenated Holey Two-Dimensional Structures. *Nat. Commun.* **2015**, *6*, No. 6486.
(50) Sahin, H. Structural and Phononic Characteristics of Nitrogenated Holey Graphene. *Phys. Rev. B* **2015**, *92*, No. 085421.
(51) Li, X.; Cui, P.; Zhong, W.; Li, J.; Wang, X.; Wang, Z.; Jiang, J. Graphitic Carbon Nitride Supported Single-Atom Catalysts for Efficient Oxygen Evolution Reaction. *Chem. Commun.* **2016**, *52*, 13233−13236.
(52) Ma, D. W.; Wang, Q.; Yan, X.; Zhang, X.; He, C.; Zhou, D.; Tang, Y.; Lu, Z.; Yang, Z. 3d Transition Metal Embedded C_2N Monolayers as Promising Single-Atom Catalysts: a First-Principles Study. *Carbon* **2016**, *105*, 463−473.
(53) Wang, Z.; Yu, Z.; Zhao, J. Computational Screening of a Single Transition Metal Atom Supported on the C_2N Monolayer for

DOI: 10.1021/acs.jpcc.8b06494
J. Phys. Chem. C 2018, 122, 19712−19721

Electrochemical Ammonia Synthesis. *Phys. Chem. Chem. Phys.* **2018**, *20*, 12835−12844.
(54) Li, X.; Zhong, W.; Cui, P.; Li, J.; Jiang, J. Design of Efficient Catalysts with Double Transition Metal Atoms on C_2N Layer. *J. Phys. Chem. Lett.* **2016**, *7*, 1750−1755.
(55) Li, F.; Chen, Z. Cu Dimer Anchored on C_2N Monolayer: Low-cost and Efficient Bi-atom Catalyst for CO Oxidation. *Nanoscale* **2018**. DOI: 10.1039/C8NR03394C.
(56) Nørskov, J. K.; Bligaard, T.; Rossmeisl, J.; Christensen, C. H. Towards the Computational Design of Solid Catalysts. *Nat. Chem.* **2009**, *1*, 37.
(57) Greeley, J.; Jaramillo, T. F.; Bonde, J.; Chorkendorff, I.; Nørskov, J. K. Computational High-Throughput Screening of Electrocatalytic Materials for Hydrogen Evolution. *Nat. Mater.* **2006**, *5*, 909.
(58) Delley, B. An All-Electron Numerical Method for Solving the Local Density Functional for Polyatomic Molecules. *J. Chem. Phys.* **1990**, *92*, 508−517.
(59) Delley, B. From Molecules to Solids with the Dmol3 Approach. *J. Chem. Phys.* **2000**, *113*, 7756−7764.
(60) Perdew, J. P.; Burke, K.; Ernzerhof, M. Generalized Gradient Approximation Made Simple. *Phys. Rev. Lett.* **1996**, *77*, 3865−3868.
(61) Grimme, S. Semiempirical GGA-type Density Functional Constructed with a Long-Range Dispersion Correction. *J. Comput. Chem.* **2006**, *27*, 1787−1799.
(62) Delley, B. Hardness Conserving Semilocal Pseudopotentials. *Phys. Rev. B* **2002**, *66*, No. 155125.
(63) Hirshfeld, F. L. Bonded-Atom Fragments for Describing Molecular Charge Densities. *Theor. Chim. Acta* **1977**, *44*, 129−138.
(64) Nørskov, J. K.; Rossmeisl, J.; Logadottir, A.; Lindqvist, L.; Kitchin, J. R.; Bligaard, T.; Jónsson, H. Origin of the Overpotential for Oxygen Reduction at a Fuel-Cell Cathode. *J. Phys. Chem. B* **2004**, *108*, 17886−17892.
(65) Peterson, A. A.; Abild-Pedersen, F.; Studt, F.; Rossmeisl, J.; Nørskov, J. K. How Copper Catalyzes the Electroreduction of Carbon Dioxide into Hydrocarbon Fuels. *Energy Environ. Sci.* **2010**, *3*, 1311−1315.
(66) Klamt, A.; Schuurmann, G. COSMO: a New Approach to Dielectric Screening in Solvents with Explicit Expressions for the Screening Energy and Its Gradient. *J. Chem. Soc., Perkin Trans. 2* **1993**, *5*, 799−805.
(67) Nie, X.; Luo, W.; Janik, M. J.; Asthagiri, A. Reaction Mechanisms of CO_2 Electrochemical Reduction on Cu(111) Determined with Density Functional Theory. *J. Catal.* **2014**, *312*, 108−122.
(68) Lim, D.-H.; Jo, J. H.; Shin, D. Y.; Wilcox, J.; Ham, H. C.; Han, S. W. Carbon Dioxide Conversion into Hydrocarbon Fuels on Defective Graphene-Supported Cu Nanoparticles from First Principles. *Nanoscale* **2014**, *6*, 5087−5092.
(69) Li, X.; Bi, W.; Chen, M.; Sun, Y.; Ju, H.; Yan, W.; Zhu, J.; Wu, X.; Chu, W.; Wu, C.; et al. Exclusive Ni−N_4 Sites Realize Near-Unity CO Selectivity for Electrochemical CO_2 Reduction. *J. Am. Chem. Soc.* **2017**, *139*, 14889−14892.
(70) Zhang, C.; Yang, S.; Wu, J.; Liu, M.; Yazdi, S.; Ren, M.; Sha, J.; Zhong, J.; Nie, K.; Jalilov, A. S.; et al. Electrochemical CO_2 Reduction with Atomic Iron-Dispersed on Nitrogen-Doped Graphene. *Adv. Energy Mater.* **2018**, No. 1703487.
(71) Pan, Y.; Lin, R.; Chen, Y.; Liu, S.; Zhu, W.; Cao, X.; Chen, W.; Wu, K.; Cheong, W.-C.; Wang, Y.; et al. Design of Single-Atom Co−N_5 Catalytic Site: A Robust Electrocatalyst for CO_2 Reduction with Nearly 100% CO Selectivity and Remarkable Stability. *J. Am. Chem. Soc.* **2018**, *140*, 4218−4221.
(72) Xiao, H.; Cheng, T.; Goddard, W. A. Atomistic Mechanisms Underlying Selectivities in C1 and C2 Products from Electrochemical Reduction of CO on Cu(111). *J. Am. Chem. Soc.* **2017**, *139*, 130−136.
(73) Goodpaster, J. D.; Bell, A. T.; Head-Gordon, M. Identification of Possible Pathways for C−C Bond Formation during Electrochemical Reduction of CO_2: New Theoretical Insights from an Improved Electrochemical Model. *J. Phys. Chem. Lett.* **2016**, *7*, 1471−1477.
(74) Ooka, H.; Figueiredo, M. C.; Koper, M. T. M. Competition between Hydrogen Evolution and Carbon Dioxide Reduction on Copper Electrodes in Mildly Acidic Media. *Langmuir* **2017**, *33*, 9307−9313.
(75) Hirunsit, P. Electroreduction of Carbon Dioxide to Methane on Copper, Copper−Silver, and Copper−Gold Catalysts: A DFT Study. *J. Phys. Chem. C* **2013**, *117*, 8262−8268.
(76) Peterson, A. A.; Nørskov, J. K. Activity Descriptors for CO_2 Electroreduction to Methane on Transition-Metal Catalysts. *J. Phys. Chem. Lett.* **2012**, *3*, 251−258.
(77) Kong, D.; Cha, J. J.; Wang, H.; Lee, H. R.; Cui, Y. First-Row Transition Metal Dichalcogenide Catalysts for Hydrogen Evolution Reaction. *Energy Environ. Sci.* **2013**, *6*, 3553−3558.
(78) Kim, K.-S.; Kim, W. J.; Lim, H.-K.; Lee, E. K.; Kim, H. Tuned Chemical Bonding Ability of Au at Grain Boundaries for Enhanced Electrochemical CO_2 Reduction. *ACS Catal.* **2016**, *6*, 4443−4448.

DOI: 10.1021/acs.jpcc.8b06494
J. Phys. Chem. C 2018, 122, 19712−19721